Cell Motility and the Cytoskeleton 49:1–15 (2001)

Centrosome and Spindle Pole Microtubules Are Main Targets of a Fluorescent Taxoid Inducing Cell Death

Miguel Abal,[1] André A. Souto,[2] Francisco Amat-Guerri,[2] A. Ulises Acuña,[3] Jose M. Andreu,[1]* and Isabel Barasoain[1]

[1]*Centro de Investigaciones Biológicas, CSIC, Madrid, Spain*
[2]*Instituto de Química Orgánica, CSIC, Madrid, Spain*
[3]*Instituto de Química-Fisica Rocasolano, CSIC, Madrid, Spain*

Microtubules offer a very large local concentration of binding sites for cytotoxic taxoids or for hypothetical endogenous regulators. Several compounds from diverse sources stabilize microtubules and arrest cell division similarly to the antitumour drug Taxol. We have investigated the subcellular location of the Taxol binding sites, employing a fluorescent taxoid (FLUTAX) that reversibly interacts with the Taxol binding sites of microtubules and induces cellular effects similar to Taxol. The specific binding of FLUTAX to a fraction of the available cellular binding sites effectively inhibits division of cultured human tumour cells at G_2/M, and triggers apoptotic death. The loci of reversible binding, directly imaged in intact U937 cells treated with cytotoxic doses of fluorescent taxoid are the centrosomes, with a few associated microtubules in interphase cells, and the spindle pole microtubules in mitotic cells, instead of uniformly labelling the microtubule cytoskeleton. Cytoskeletal lesions induced and visualized with FLUTAX consist of microtubule bundles and abnormal mitoses, including monopolar spindles and highly fluorescent multipolar spindles. The multiple asters and monopolar spindles mark arrested U937 leukaemia and OVCAR-3 ovarian carcinoma cells on their path to apoptosis (as well as K562, HeLa, and MCF-7 cells). Depending on the FLUTAX treatment, OVCAR-3 cells died from abnormal mitosis or from a subsequent interphase with double chromatin content and lobulated nuclei (micronuclei), indicating impairment of centrosome separation. Fragmented centrosomes could be observed in FLUTAX-treated non-transformed 3T3.A31 cells, which developed micronuclei but were resistant to apoptosis. These results strongly suggest that centrosomal impairment by taxoid binding during interphase, in addition to the suppression of the kinetochore microtubule dynamics in the mitotic spindle, is a primary cause of cell cycle de-regulation and cell death. Cell Motil. Cytoskeleton 49:1–15, 2001.

Key words: Taxol; fluorescent probes; intact tumour cells; microtubule cytoskeleton

Contract grant sponsor: Fundación Científica de la Asociación Española contra el Cancer; Contract grant sponsor: Direccion General de Investigación; Contract grant numbers: BIO99-0859-C03-02, PB96-852, APC96-0071; Contract grant sponsor: Comunidad Autonoma de Madrid. Contract grant number: CAM 07B/0025/1999.

Miguel Abal's present address is Institut Curie, Section Recherche, UMR 144/CNRS, 26 rue d'Ulm, 75248 Paris Cedex 05, France.

André A. Souto's present address is Universidade Pontificia Catolica do Rio Grande do Sul, 90619-900, Porto Alegre-RS, Brasil.

*Correspondence to: J.M. Andreu, CIB, CSIC, Velazquez 144, 28006 Madrid, Spain. E-mail: j.m.andreu@cib.csic.es.

Received 25 August 2000; Accepted 27 December 2000

INTRODUCTION

The centrosome of animal cells is a unique organelle that nucleates and organizes microtubules for important cellular functions including the segregation of chromosomes by the mitotic spindle, cellular architecture, and cytoplasmic transport [Paoletti and Bornens, 1997; Zimmerman et al., 1999]. Microtubule-organizing proteins cluster at the centrosome [Chang and Stearns, 2000]. Central to microtubule function is their dynamics, which is suppressed by Taxol (paclitaxel), a natural diterpenoid that blocks cell division and triggers cell death [Horwitz, 1992; Suffness, 1995; Sorger et al., 1997; Jordan and Wilson, 1998]. Taxol is widely used as a microtubule stabilizing agent and employed in the treatment of ovarian, breast, lung, head and neck, cervix carcinomas and lymphomas [Rowinsky and Donehower, 1995].

Taxol induces the in vitro assembly of microtubules from αβ-tubulin dimers [Schiff et al., 1979; Andreu et al., 1992; Díaz et al., 1996], encompassing the binding of one drug molecule per assembled tubulin dimer [Horwitz, 1992, Díaz and Andreu, 1993]. Taxol binding and microtubule elongation are linked reactions, probably coupled by the participation of Taxol in a lateral contact between protofilaments [Díaz et al., 1993; Andreu et al., 1994]. In the electron crystallography model structure of tubulin dimers in zinc-induced sheets stabilized with Taxol [Nogales et al., 1998], the Taxol binding site is located between the β-tubulin core helix H7 and the M loop, which makes lateral contact with the neighbouring protofilament. The α-tubulin zone equivalent to Taxol is occupied by a loop of the peptide chain. From the docking of this tubulin structure into microtubules [Nogales et al., 1999], Taxol surprisingly faces the microtubule lumen. However, the Taxol binding site of preassembled microtubules is easily accessible to the reversible binding of taxoids, making a puzzle of how Taxol might reach the microtubule lumen at such a high rate [Evangelio et al., 1998; Díaz et al., 1998]. In fact, the fast kinetics of binding of fluorescent Taxol derivatives indicates that the Taxol binding site is directly accessible from the microtubule surface [Díaz et al., 2000]. The Taxol binding site of microtubules includes β-tubulin-photoaffinity labeled residues in the 1–31 and 217–231 sequences and Arg 282 [Rao et al., 1994, 1995, 1999]. Resistance to Taxol has been associated to point mutations in β-tubulin residues Phe270, Thr274, Arg 282, and Ala364 in human ovarian cancer cell lines [Giannakakou et al., 1997, 2000a], in β-tubulin residues 4, 147, 180, 183 and 260 in non-small-cell lung cancer biopsies [Monzó et al., 1999], and in a β-tubulin leucine cluster (Leu-215, Leu-217 and Leu-228) in hamster ovary cells [Gonzalez-Garay et al., 1999].

Taxol may induce cell death by diverse mechanisms. Cytoplasmic microtubules of PtK1 epithelial cells abruptly disassemble into tubulin at the G_2/M transition, immediately after the nuclear envelope breakdown, and repolymerize in the spindle [Zhai et al., 1996], offering a potential point of Taxol-induced microtubule stabilization and cycle blockage. Taxol-induced stabilization and massive assembly of cellular microtubules [Schiff and Horwitz, 1980; De Brabander et al., 1981] were first thought to be responsible for the inhibition of cell division by this drug. However, it has been shown that low concentrations of Taxol inhibit the growth of HeLa and other human tumor cells by kinetically suppressing microtubule dynamics, similarly to the microtubule inhibitors colchicine and vinblastine [Jordan et al., 1993; Yvon et al., 1999]. Blocking at the metaphase/anaphase spindle checkpoint results in abnormal mitotic exit and apoptotic HeLa cell death [Jordan et al., 1996; Derry et al., 1998]. Taxol treatment of PtK1 cells suppresses tension at the kinetochores, inducing a re-phosphorylation of epitope 3f3/2, and also some unattached kinetochores that accumulate the protein Mad2 [Waters et al., 1998], which in turn inhibits the anaphase promoting complex [Gorbsky et al., 1998]. In contrast, Taxol was reported to inhibit spindle formation in colon carcinoma cells [Long and Fairchild, 1994). Taxol and other microtubule drugs induce mitotic arrest, Bcl2 protein phosphorylation in cancer cells, and apoptosis [Haldar et al., 1998, Srivastava et al., 1998, Fang et al., 1998].

The Taxol binding site interacts as well with several chemically unrelated antitumour compounds from diverse sources that stabilize microtubules, including the epothilones [Bollag et al., 1995], discodermolide [ter Haar et al., 1996], eleutherobin [Long et al., 1998], and laulimalide [Mooberry et al., 1999]; several of them share a common pharmacophore [Ojima et al., 1999; He et al., 2000; Giannakakou et al., 2000a]. Therefore, it may be asked if these are defensive toxic molecules generated by convergent evolution, whether there is a more fundamental biological role of the Taxol binding site of microtubules, and if this site might recognize endogenous cellular regulators that are mimicked by Taxol [Schiff et al., 1979; Suffness, 1994]. Another important question is whether Taxol is preferentially recognized by certain microtubules, or by other cellular components. Although Taxol is believed to bind to cellular microtubules [Parness and Horwitz, 1981], the subcellular targets of cytotoxic Taxol binding have not yet been directly visualized. Some of its numerous effects may be microtubule-independent, such as in mouse macrophages [Wolfson et al., 1997; Bhat et al., 1999] or the in vitro interaction with Bcl2 [Rodi et al., 1999].

We have asked which are the main cellular binding sites that recognize Taxol, block cell division, and trigger

cell death. It is shown here that centrosomes and spindle microtubules contain such sites, which have been directly determined employing a specific fluorescent taxoid probe.

MATERIALS AND METHODS

Fluorescent Taxoids

Conjugation through the free amino group of 7-*O*-(L-alanyl)taxol with amine-reactive dyes was employed as a general method designed to prepare bioactive derivatives, such as 7-*O*-[*N*-(4′-fluoresceincarbonyl)-L-alanyl]taxol (FLUTAX) [Souto et al., 1995]. The fluorescein, anchored to alanine at the non-essential position 7 of Taxol, displays motion relative to the taxane moiety, which is restricted in the microtubule-bound taxoid [Evangelio et al., 1998]. On the other hand, conjugation with 2′-acetyl-7-(L-alanyl)taxol gave the inactive compound 2′-*O*-acetyl-7-*O*-[*N*-(4′-fluoresceincarbonyl)-L-alanyl]taxol (2′-Ac-FLUTAX) [Jimenez-Barbero et al., 1998] designed for control experiments. FLUTAX is able to induce the assembly of GDP-bound tubulin as Taxol does. FLUTAX competes with Taxol for binding to one site per tubulin dimer assembled into microtubules, [Evangelio et al., 1998]. FLUTAX allows direct microscopy of microtubules in permeabilized cells, similarly to the derivative with fluorine atoms in positions 2 and 7 of the fluorescein moiety (FLUTAX-2) [Díaz et al., 2000], and more specifically than the rhodamine analog 7-*O*-[*N*-(4′-tetramethylrhodaminecarbonyl)-L-alanyl]taxol (ROTAX) and other taxoids conjugated with different fluorophors [Evangelio et al., 1998]. Docetaxel (the common name for Taxotere) displaces FLUTAX from cellular microtubules. Docetaxel was preferred to Taxol in most FLUTAX displacement controls because it is a closely related compound that binds to the same microtubule site and it has larger solubility and affinity than Taxol [Díaz and Andreu, 1993].

Cells and Culture Conditions

U937 monocytic human leukemia and K562 human myelocytic leukemia cells were grown as described [De Inés et al., 1994]. MCF-7 human breast carcinoma and OVCAR-3 human ovary adenocarcinoma cells (American Type Culture Collection, Rockville, MD; ATCC) were, respectively, cultured in Minimum Essential Eagle's medium (MEM) -10% fetal calf serum (FCS) and Dulbecco's modified MEM (DMEM) - 20% FCS -10 mM N-2-hydroxyethylpiperazine-N-2′-ethanesulfonic acid (Hepes), both supplemented with 0.1 mM non-essential amino acids, 1.0 mM sodium pyruvate, and 10 μg/ml bovine insulin. HeLa S3 human epithelioid cervix carcinoma cells (ATCC), 3T3.A31 murine embryonic fibroblasts (ATCC), and PtK2 potoroo epithelial-like kidney cells (ATCC) were grown in monolayer in DMEM-10% FCS [De Inés et al., 1994]. OVCAR-3 cells were synchronized by a double blockage with thymidine excess, accumulating cells in G_1/S transition [Bootsma et al., 1964]. Cells were first incubated with 2 mM thymidine for 24 h (cells in G_2/M and in G_1 phases progress to G_1/S and those in S are blocked). They were washed and cultured in fresh medium for an additional 16 h (cells in S reach G_1 and cells in G_1/S pass S phase). Cells were incubated again with 2 mM thymidine during 24 h to block them in G_1/S, washed, placed in fresh medium, and cultured for 18 h before use, reaching G_1. 3T3.A31 cells were synchronized by serum deprivation [Campisi et al., 1984], by incubation in culture medium - 0.5 % FCS during 36 h, which blocks them at the G_0/G_1 transition, and used 6 h after being supplemented with 10% FCS, reaching G_1.

Cellular Incorporation of Fluorescent Taxoid, Flow Cytometry, and Cell Death

Cells (150,000 per ml) were treated with FLUTAX. The fluorescent taxoid content of intact cells excluding propidium iodide (50 μg/ml, Sigma) was determined with a Coulter Epics XL flow cytofluorometer. Five thousand cells were counted in the 525-nm fluorescein emission channel; non-specific binding was determined by adding the non-fluorescent taxoid docetaxel in a 50-fold excess relative to FLUTAX. Progression through the cell cycle was monitored in identical culture aliquots by flow cytometry DNA determination, after propidium iodide staining of Nonidet P40-permeabilized cells [De Inés et al., 1994]. The chromatin structure was examined by assaying the sensitivity of DNA to in situ acid denaturation as described [Darzynkiewicz, 1994], with minor modifications. Rehydrated fixed cells (10^6 cells in 0.1 ml) were incubated with RNAse A (1 Kunitz U, 1 h at 37°C), directly treated with 0.4 ml of 0.1 M HCl (30 sec, room temperature), stained with 1.5 ml of acridine orange (Merck, 6 μg/ml), and measured by flow cytometry.

Cytosolic fragmented DNA was isolated and electrophoresed as described [Mollinedo et al., 1993], employing a 123-bp DNA ladder (Life Technologies, Inc., Gaithersburg, MD) as standard. Cells with fragmented nuclei were counted in cultures stained with Hoescht 33342. Plasma membrane rupture was detected by propidium iodide nuclear staining.

Cellular Incorporation of ^{3}H-Taxol

Cells were plated in 24-well plates and incubated for 16 h with different concentrations of ^{3}H-Taxol. ^{3}H-Taxol (>3 Ci/mmol) was a gift from Drs. I. Ringel and S.B. Horwitz, kept in methanol solution at −70°C and its purity checked by HPLC [Díaz and Andreu, 1993], and also from Moravek Biochemicals (Brea, CA). The binding of labelled ligand to the cells was determined by

centrifugation and scintillation counting, and normalized by the actual cell number in each well. The nonspecific binding of ^{3}H-Taxol was determined by incubating cells with the same concentrations of radiolabelled Taxol plus a 50-fold excess of docetaxel. The specific binding is obtained by subtracting the nonspecific from the total binding.

Fluorescence Microscopy

Direct images of living cells labelled with fluorescent taxoid, Hoechst 33342 (0.05 μg/ml, Sigma) and excluding propidium iodide (1 μg/ml, Sigma) in culture medium were acquired by epifluorescence microscopy with Zeiss 63x Plan-Neofluar or 100x Plan-Apochromat objectives and Axioplan microscopes; the images were recorded with Photometrics 200 KAF-1400 and Hamamatsu 4742-95 cooled CCD cameras, IPLab Spectrum, and HiPic software, respectively, and printed using Adobe Photoshop [Evangelio et al., 1998]. Indirect immunofluorescence was performed as described [De Inés et al., 1994; Evangelio et al., 1998]. Microtubules were visualized with DM1A mouse monoclonal antibody (Sigma, diluted 1/400) or with C85 rabbit monospecific antibodies to α-tubulin [Andreu et al., 1988], and γ-tubulin was detected with monoclonal antibodies TU-30 [Nováková et al., 1996] (diluted 1/8) or GTU-88 (Sigma, diluted 1/10,000). Polyglutamylated α- and β-tubulin was detected with GT-335 monoclonal antibody [1/10,000], which stains centrioles in non-neuronal cells [Wolff et al., 1992; Paoletti et al., 1997; Bobinnec et al., 1998]. In FLUTAX and γ-tubulin colocalization experiments U937 cells were centrifuged onto poly-lysine treated CELLocate coverslips (Eppendorf), first imaged alive placing the coverslip in a sealed chamber and then fixed with methanol and processed for immunofluorescence with anti-γ-tubulin antibodies and rhodamine-conjugated secondary antibodies (controls were made omitting FLUTAX or the antibodies to γ-tubulin).

RESULTS

Binding of Fluorescent Taxoid, Cell Cycle Arrest, and Cell Death

We first asked whether the Taxol binding sites of relevant intact cells would interact with the fluorescent taxoids and if their effects would be similar to Taxol. To these purposes, we employed U937 human monocytic leukaemia and OVCAR-3 ovarian carcinoma cells, and other cell lines for comparisons or as controls. We knew that the fluorescent derivative FLUTAX can replace Taxol in vitro assembled microtubules and allows direct microscopy of the microtubule cytoskeleton in permeabilized cells [Evangelio et al., 1998]. Fluorescent Taxol uptake by cells cultured in suspension was measured by flow cytometry (Fig. 1A). FLUTAX is specifically bound by U937 cells in a saturable manner (Fig. 1B); similar results were obtained with OVCAR-3 cells (see below; see also Fig. 3A) and with K562 myelocytic leukaemia and MCF-7 mammary carcinoma cells (not shown). As with Taxol, FLUTAX induces the accumulation of U937 cells in the G_2/M phases of the cell cycle as well as apoptotic cell death, evidenced by nuclear fragmentation (Fig.1E) and an internucleosomal pattern of DNA cleavage (Fig. 1F). The cell cycle half-inhibitory concentration of the taxoids (Table I) indicates that ROTAX is about 2-fold and FLUTAX is about 20-fold less active than Taxol on the cells tested. 2′-Ac-FLUTAX has a 500-fold weaker activity, and fluorescein-alanine (the non-taxoid moiety of FLUTAX) was inactive at comparable concentrations (Table I). The weak residual activity of 2′-Ac-FLUTAX is probably the result of the slow hydrolysis of the 2′-acetyl group in the serum-containing culture medium, rendering the free 2′-OH of the Taxol side chain essential for recognition by cellular microtubules [Jimenez-Barbero et al., 1998]. ROTAX gave a non-specific vesicular staining in PtK2 cytoskeletons [Evangelio et al., 1998] in comparison with the labelling by FLUTAX (see Fig. 4D). This cast doubt on whether the powerful inhibition of cell division by ROTAX (Table I) is specific of Taxol binding sites. Therefore, FLUTAX was predominantly employed for this study, although it has a weaker cytostatic activity than ROTAX. Similarly to Taxol, treatment of PtK2 cells with FLUTAX (at 20-fold larger concentration) induced microtubule disorganization, with characteristic microtubule bundles and multiple asters, which were detected by immunofluorescence with antibodies to tubulin (not shown).

Comparison of the cell cycle effects of FLUTAX with its binding to U937 leukaemia cells as a function of total probe concentration (Fig. 2A) shows that half maximal cell cycle arrest takes place at low taxoid concentrations ($\leq$ 50 nM FLUTAX), corresponding to a specific fractional binding of approximately 10% of the available binding sites (assuming FLUTAX binding to be roughly proportional to the cell-associated fluorescence intensity measured by flow cytometry; the values for K562, OVCAR-3, and MCF-7 cells were 30, 35, and 52%, respectively). The FLUTAX binding and U937 cell cycle arrest (Fig. 2A) paralleled similar results with Taxol, in which a few percent specific binding of isotopically labelled ^{3}H-Taxol similarly arrested U937 cells, at one order of magnitude lower drug concentrations than FLUTAX (see Fig. 2B and inhibition by FLUTAX). A second stage of binding (50–200 nM FLUTAX, Fig. 2A) coincided with the accumulation of apoptotic U937 cells

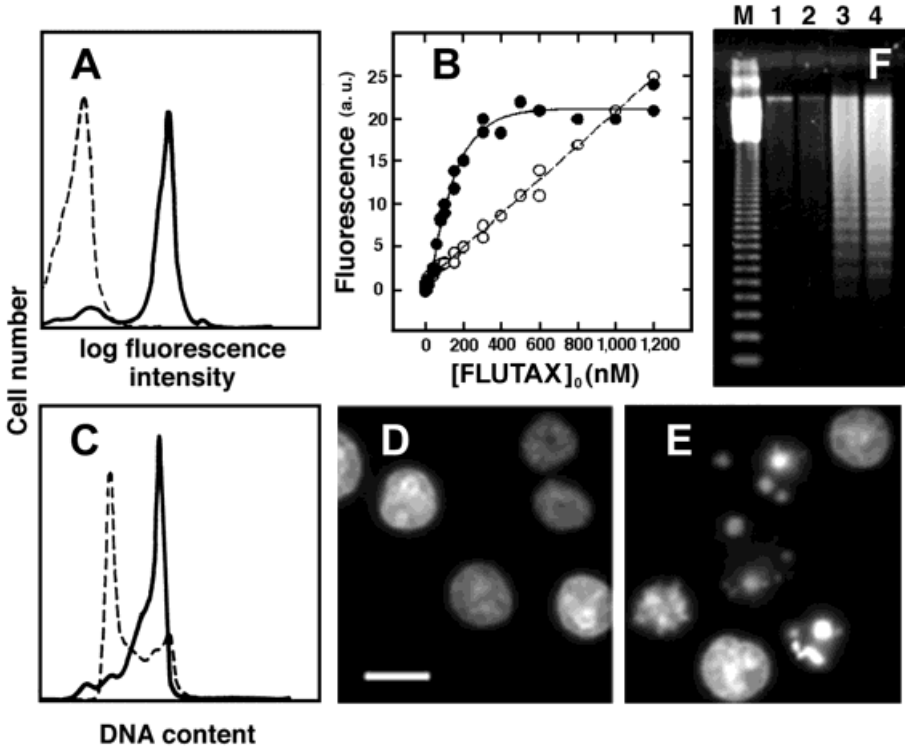

Fig. 1. Cellular incorporation and effects of fluoresceinated Taxol (FLUTAX; for the chemical structures of this compound and Taxol, see fig. 1 in Evangelio et al. [1998]). **A:** U937 cells were incubated with 80 nM FLUTAX (16 h), and the taxoid uptake by intact cells was determined by flow cytometry (fluorescein emission), shown by the continuous line (the *dashed line* is the background of untreated cells). **B:** Specific binding (total minus non-specific binding; *solid circles*) and non-specific binding (cells incubated with an added 50-fold excess of docetaxel; *open circles*) vs. total FLUTAX concentration (the results of two experiments have been plotted together). **C:** Cell cycle profiles in aliquots of the same cultures as in A in which the DNA content has been determined with flow cytometry (propidium iodide emission). **D:** U937 cells stained with Hoechst 33342 (5 min) and observed by fluorescence microscopy (bar = 10 μm); **E:** U937 cells incubated with 80 nM FLUTAX (16 h) and stained with Hoechst 33342. **F:** Electrophoresis of DNA from the FLUTAX-treated U937 cells. Lane M: 123-bp DNA ladder markers. Lanes 1–4: U937 cells incubated with 0, 50, 80, and 200 nM FLUTAX (16 h), respectively.

TABLE I. Cell Cycle Half-Inhibitory Concentration (nM) of Taxol and Fluorescent Derivatives*

	U937	K562	OVCAR-3	MCF-7	HeLa	3T3.A31	PtK2
Taxol	2.6 ± 0.2	13.8 ± 4.3	3.5 ± 0.4	4.4 ± 0.8	4.6 ± 0.3	40.4 ± 2	430 ± 20
FLUTAX	49 ± 6	272 ± 27	65 ± 1	92 ± 12	104 ± 3	330 ± 10	8,300 ± 1,000
ROTAX	5.1 ± 0.3	21 ± 2	nd	nd	nd	nd	440 ± 10
2′-Ac-Flutax	1,400 ± 500	3,800 ± 700	nd	nd	nd	nd	nd
Flu-Ala	>2,500	>5,000	nd	nd	nd	nd	nd

*The half inhibitory concentrations were determined from the half maximal increase of the percent cells in G_2/M and the half maximal decrease of cells in G_0/G_1 phases (see Fig. 2A,B). A minimum of two separate experiments was performed with each cell line. The numbers given are the average and standard error. Different incubation times were employed to obtain mitotic arrest, depending on the duration of each cell cycle (compare Fig. 2C with Fig. 3A) (U937 and K562 cells, 16 h; HeLa, 20 h; PtK2, 24 h; 3T3.A31, 36 h; OVCAR-3 and MCF 7, 40 h). Practically the same results were obtained with U937 and K562 cells by counting the number of cells relative to untreated controls after 24 h of growth (nd: non determined). Flu-Ala, N-(4′-fluoresceincarbonyl)-L-alanine.

(Fig. 2D). The fraction of U937 cells with double DNA content (G_2/M phases) gradually increased from 25% in the untreated cultures to 80% in the FLUTAX-arrested cultures (Fig. 2A,C). Binding of FLUTAX is reversible, since it is released from washed U937 cells in fresh culture medium with a half-life of approximately 6 h (Fig. 2E). It was concluded from these experiments that the reversible, specific interaction of FLUTAX with a fraction of the Taxol binding sites causes cell cycle arrest and death effects akin to Taxol in the cells examined. FLUTAX was, therefore, employed to investigate the location of the cellular structures presenting Taxol bind-

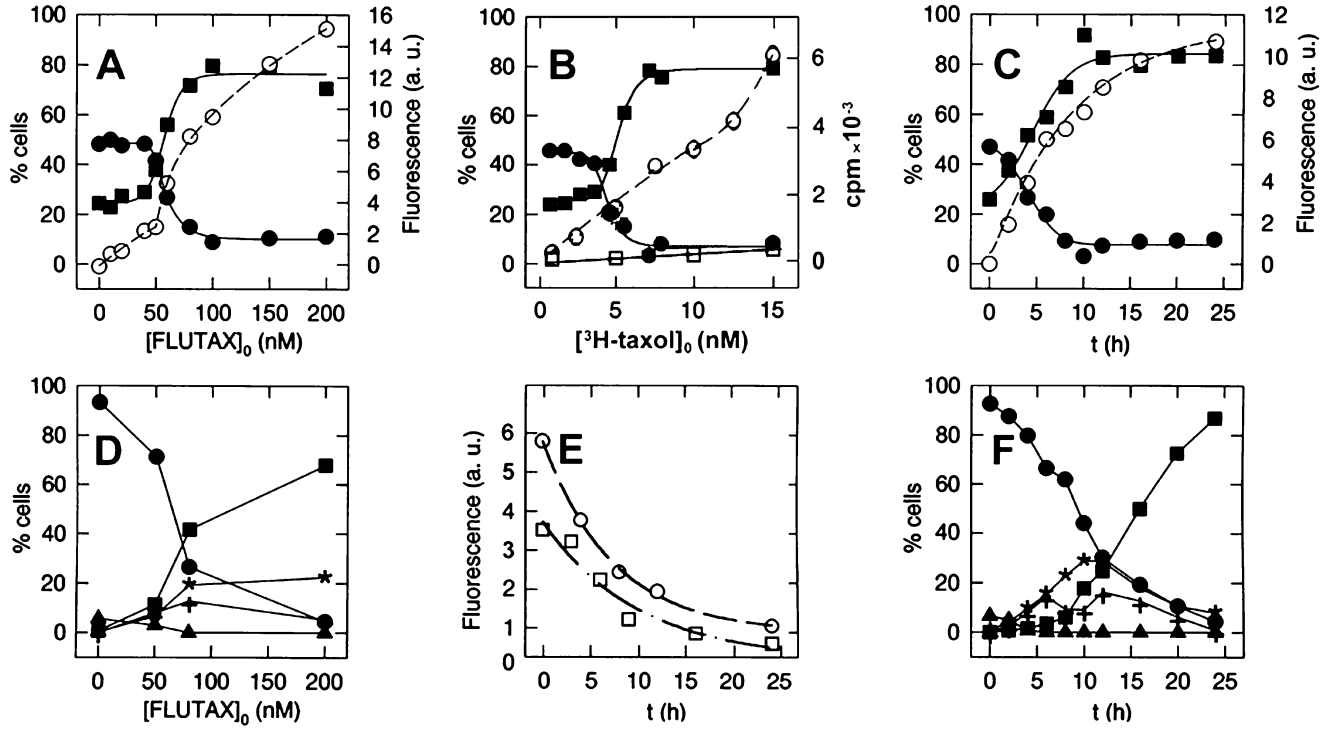

Fig. 2. FLUTAX binding and effects on U937 cells. **A:** Concentration dependence of specific FLUTAX uptake (*open circles*, expressed as fluorescein emission) and of its action on the cell cycle (expressed as percent of cells in each zone of the flow cytometer profiles after 16 h treatment; *open circles*, specific FLUTAX binding; *closed circles*, cells in G_1; *closed squares*, cells in G_2/M). **B:** Similar experiment made with ^{3}H-Taxol (*open circles*, specific Taxol uptake, expressed as counts per minute; *open squares*, specific Taxol uptake in the presence of a 2,000-fold excess of FLUTAX; see Materials and Methods). **C:** Time course with 80 nM FLUTAX (symbols as in A and B). **D:** Fraction of interphase (*closed circles*), normal mitosis (*closed triangles*), abnormal mitosis (including detached or asymmetrically distributed chromosomes and monopolar mitoses, +) (see Fig. 4), multiple asters (*) and apoptotic cells (*closed squares*) (300 cells per point were counted by microscopic observation of their chromatin stained with Hoechst 33342). **E:** Dissociation of FLUTAX from cells incubated 16 h with 80 nM FLUTAX (*open circles*) or 1 h with 260 nM FLUTAX (*open squares*), washed twice with fresh medium and incubated the indicated periods, and measured with flow cytometry. **F:** Time-course of cellular effects of 80 nM FLUTAX (symbols as in D). In each panel, the values shown are one representative experiment out of three performed.

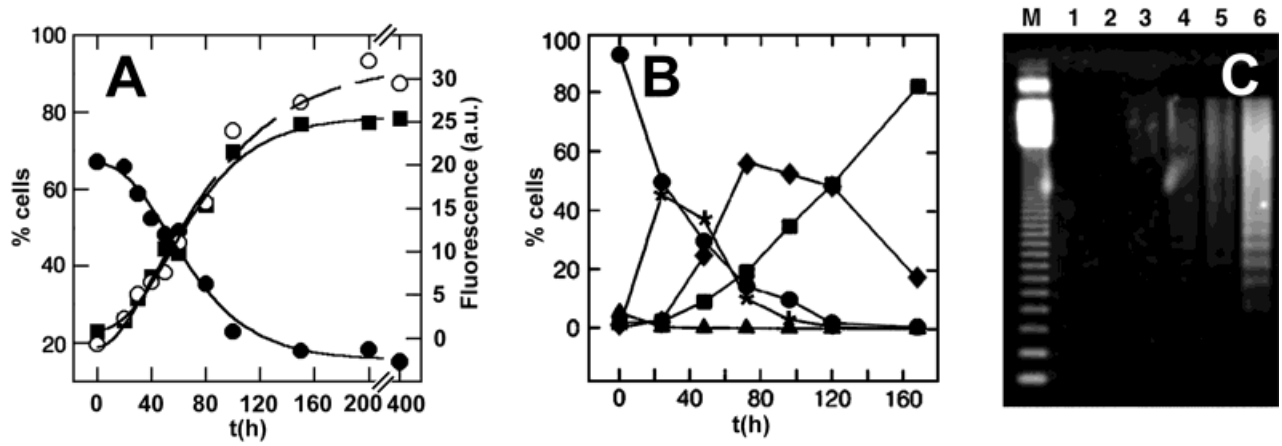

Fig. 3. Time courses of FLUTAX binding and effects on OVCAR-3 cells. **A:** FLUTAX binding and effects on the cell cycle (150 nM FLUTAX; *closed circles*, cells in G_1; *closed squares*, cells in G_2/M; *open circles*, specific FLUTAX binding). **B:** Percent of normal interphase (*closed circles*), mitosis (*closed triangles*), multiple asters, and other abnormal mitoses (*), micronucleated (*closed diamonds*), and apoptotic (*closed squares*) cells, counted with Hoescht 33342-stained chromatin (see Fig. 2A,F). **C:** Electrophoretic analysis of DNA fragmentation. Lane M: 123-bp DNA ladder markers; lanes 1–6: cells treated with 150 nM FLUTAX during 0, 16, 24, 48, 72, and 96 h, respectively.

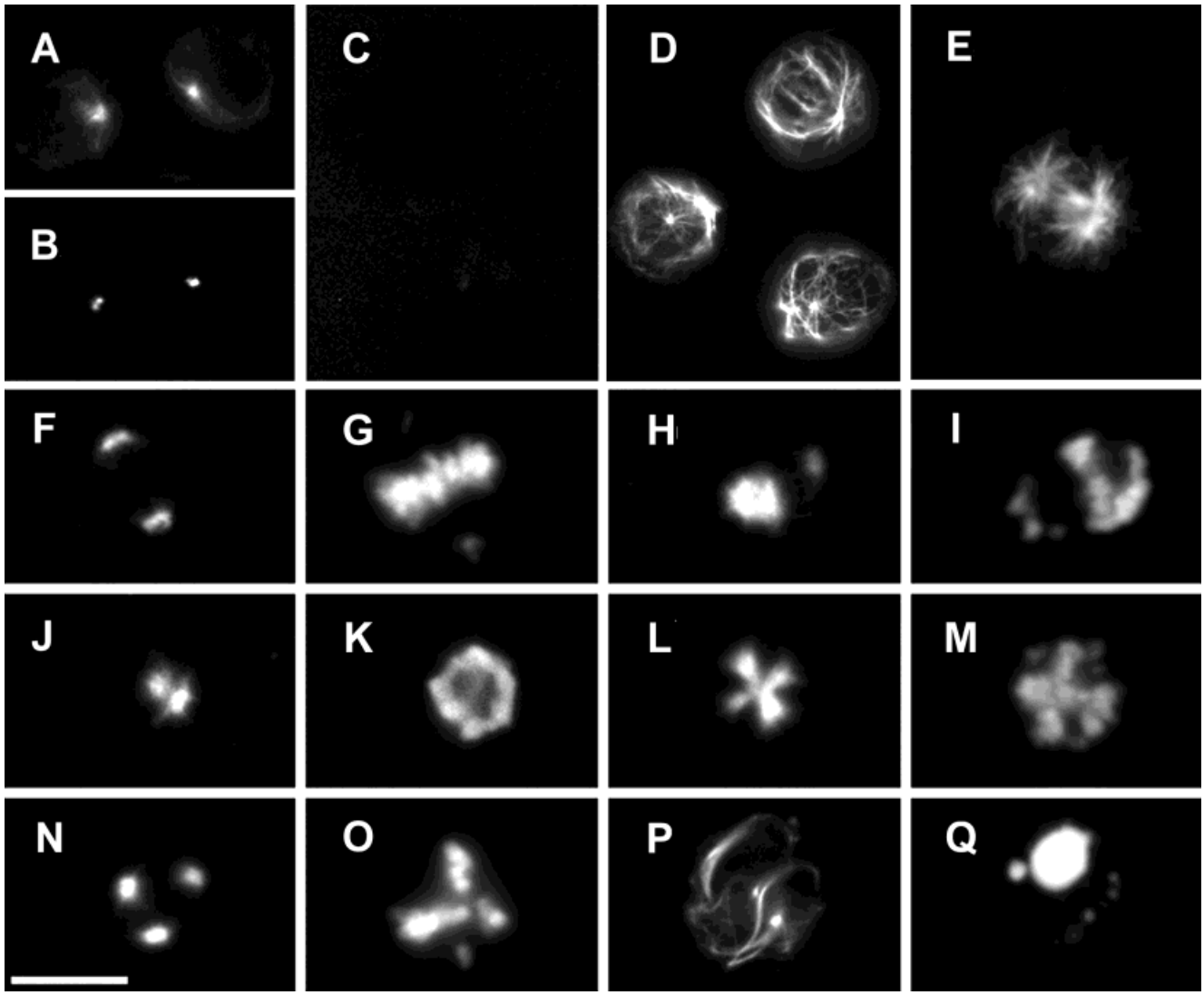

Fig. 4. Representative images of FLUTAX binding to intact U937 cells. Cells were incubated with growth inhibitory concentrations of FLUTAX (50 and 80 nM; 16 h) and the subcellular distribution of the taxoid directly imaged under the fluorescence microscope. **A:** Interphase cells. **B:** γ-tubulin staining of the same cells (see Materials and Methods). **C:** Mitotic and interphase cells were processed as in A but a 50-fold excess of the non-fluorescent taxoid docetaxel was added during the last 4 h of incubation that erased the fluorescence. **D:** Microtubule cytoskeleton of permeabilized cells as compared to A. **E:** Microtubules of a mitotic cell visualized by indirect immunofluorescence, to be compared with FLUTAX labelling (F). Individual cells were imaged with FLUTAX through the fluorescein channel (**F,H,J,L,N,P**) and their chromatin visualized with Hoechst 33342 through the ultraviolet channel of the fluorescence microscope (**G,I,K,M,O,Q**). Cells F–I illustrate abnormal bipolar mitoses, J–M monopolar spindles, N–O multiple asters, and P,Q a dying cell with microtubule bundles (200 nM FLUTAX). Bar = 10 μm.

ing sites and the effects of ligation of these sites on the cell cycle.

The FLUTAX-arrested U937 cell cultures consisted of a transient accumulation of abnormal mitoses and multipolar spindles, with the maximum after 10–12 h of treatment with 80 nM FLUTAX, where the proportion of normal mitosis was insignificant. This was followed by the accumulation of apoptotic cells (Fig. 2D,F), with a lag time of about 10 h relative to that of cells with double DNA content (Fig. 2C). These results suggested that the taxoid-treated U937 cells arrested in aberrant mitosis develop apoptosis, without excluding the possibility that cells may die in the G_2 phase. Tumour cells may also undergo aberrant mitosis, enter the next G_1 phase with an abnormal DNA content and then die. FLUTAX-treated OVCAR-3 ovarian carcinoma cells accumulated with double DNA content (Fig. 3A). In this case, a peak of 45% abnormal mitotic cells was clearly

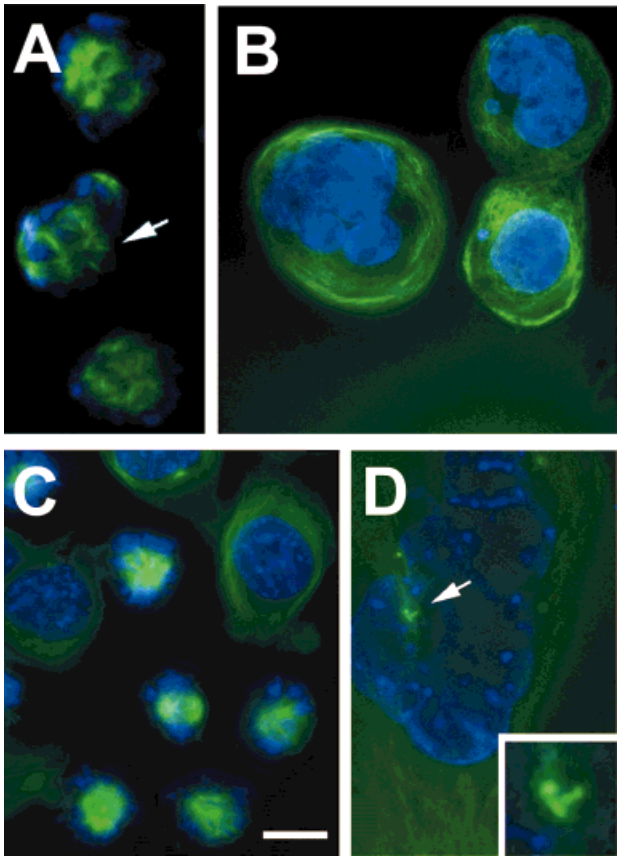

Fig. 5. Abnormal mitotic images and lobulated interphase nuclei in OVCAR-3 (**A,B**) and synchronized 3T3.A31 cells (**C,D**) treated with cytotoxic concentrations of FLUTAX. OVCAR-3 cells were treated with 150 nM FLUTAX during 40 h (A; the arrow marks a multipolar aster) and 72 h (B). Synchronized 3T3.A31 cells (6 h after the G_0/G_1 block release) were treated with 1 μM FLUTAX for 16 h (C) and 24 h (D, the *arrow* marks the centrosome). **Inset** (D): A centrosomal zone is shown magnified. DNA was stained with Hoechst 33342. Coverslip-attached cells were permeabilized by mounting them with glycerol solution, allowing extensive labelling of their microtubule cytoskeleton with the residual FLUTAX in the preparation [Evangelio et al., 1998]. Bar = 10 μm, except for D (5 μm) and its inset (1.5 μm)

followed by a second peak of 55% new interphase with lobulated nuclei (micronuclei) (Fig. 3B), which had not been observed in U937 cells. Micronucleated OVCAR-3 cells underwent massive apoptosis, not excluding the possibility of apoptosis from mitotic cells (Fig. 3B,C). MCF7 mammary carcinoma cells, HeLa, and K562 behaved similarly to OVCAR-3 cells (not shown).

Subcellular Location of the Binding Sites of Cytotoxic Fluorescent Taxoid

We inquired which are the subcellular locations of the sites of binding of fluorescent taxoid at cytotoxic doses, whether these sites are evenly distributed throughout the microtubule cytoskeleton or localized at certain microtubules, or even at non-microtubule structures. Such binding events should be the first steps leading to taxoid-induced tumour cell death. Spindles and centrosomes had been previously visualized in growing U937 cells employing a subinhibitory concentration of FLUTAX as a cytoskeletal probe [Evangelio et al., 1998]. In the present work, cells treated with growth inhibitory concentrations of FLUTAX were observed intact (non-permeabilized, possibly accumulating the taxoid) in their culture medium by fluorescence microscopy. In interphase U937 cells, FLUTAX labels the centrosomal area and barely a few microtubules, but is insignificantly bound by the rest of the cytoplasmic microtubules (Fig. 4A). The centrosomal FLUTAX labelling colocalizes with γ-tubulin (Fig. 4B). FLUTAX labelling is specific, since it is efficiently displaced by a docetaxel excess, leaving an insignificant background (Fig. 4C). Cytoplasmic microtubules and centrosomes could be observed with FLUTAX when U937 cells were permeabilized (Fig. 4D). It can be concluded that the spot labelling observed in Figure 4A most probably corresponds to FLUTAX binding by the centrosomal complex (instead of being due to the confluence of the more weakly labelled microtubules in the centrosomal area). Centrosomal labelling with FLUTAX in permeabilized PtK2 cells has also been shown to co-localize with γ-tubulin and it frequently consists of two close spots in interphase cells, probably the centrioles [see fig. 7 in Evangelio et al., 1998]. In mitotic U937 cells, instead of uniformly labelling all the spindle microtubules as with anti-tubulin antibodies (Fig. 4E), FLUTAX intensely labels the spindle pole regions (Fig. 4F). Similar labelling patterns were obtained if cell growth was inhibited with a 1-h pulse of 260 nM FLUTAX; it is of interest that when these cells were washed and placed in fresh culture medium the images of centrosomes and spindles progressively disappeared in 6 to 9 h, and could not be detected 24 h later (not shown), consistent with the FLUTAX dissociation measured with flow cytometry (Fig. 2E). ROTAX also labelled centrosomes and spindles in treated U937 cells, but gave as well a non-specific interfering cytoplasmic background.

Multiple Microtubule Asters, Microtubule Bundles, and Multiple Centrosomes Induced and Imaged With Fluorescent Taxoid

U937 cells treated with growth inhibitory concentrations of FLUTAX yield the following mitotic patterns: bipolar spindles with one or more detached chromosomes (Fig. 4F,G), spindles with chromosomes asymmetrically distributed at two poles (Fig. 4H,I), monopolar spindles surrounded by chromosomes (Fig. 4J–M), multipolar spindles (multiple asters) (Fig. 4N,O), and a negligible proportion of normal mitotic spindles. Monopolar spindles and multiple asters were the most frequent ab-

normal mitotic features imaged with FLUTAX in intact U937 cells. Images similar to the FLUTAX-treated U937 cells were also obtained with intact K562 cells, and weaker images were obtained from intact OVCAR-3, MCF-7, and HeLa cells. Abnormal mitotic images, particularly multiple asters, were observed in FLUTAX-treated permeabilized OVCAR-3 cells (Fig. 5A) and 3T3.A31 cells (Fig. 5C) as well as in K562, HeLa, and MCF-7 cells (not shown). Multiple asters stained for α-tubulin (detected with rabbit polyclonal antibodies) while only two of their poles contained γ-tubulin (detected with TU30 antibody), indicating that the rest of the poles were not associated to centrosomes (results not shown).

On the other hand, microtubule bundles were typically observed at higher doses of FLUTAX in U937 cells. Sixty-eight percent of cells treated with 200 nM FLUTAX during 16 h lacked a normal microtubule network organized from the centrosome, but presented instead microtubule bundles and had ruptured plasma membranes (Fig. 4P), 28% displayed abnormal mitosis, 4% were in interphase without bundles, and less than 1% of cells had bundles and intact plasma membranes. Microtubule bundles were observed in FLUTAX-treated permeabilized OVCAR-3 cells before undergoing apoptosis (Fig. 5B).

When OVCAR-3 cells exit from FLUTAX-induced abnormal mitosis (Fig. 5A), they form micronucleated interphase cells (Fig, 5B), suggesting impairment of centrosome separation at the previous G_2/M transition. Multiple centrosomes could be detected in FLUTAX-treated micronucleated 3T3.A31 and PtK2 cells, employing the fluorescent taxoid, antibodies to γ-tubulin and to glutamylated tubulin (not shown). Centrosome fragmentation occurs in one cell cycle, as shown with 3T3.A31 cultures synchronized in G_1 phase and then incubated with FLUTAX, which give cells in abnormal mitosis at 16 h (Fig. 5C) and micronucleated interphase cells at 24 h (Fig. 5D). The appearance of multiple or fragmented centrosomes (inset in Fig. 5D) occurs in the micronucleated interphase, after 24-h incubation.

Cells Treated With Fluorescent Taxoid Die From Mitotic Block or After Aberrant Mitotic Exit

The different cell cycle response patterns to FLUTAX treatment were further investigated by flow cytometry of acid-treated cells with acridine orange [Darzynkiewicz,1994]. With this method, the fluorescence of the probe shifts to the red with chromatin condensation, thus distinguishing the G_2 from the M phase and apoptotic chromatin (Fig. 6). FLUTAX-treated U937 cells transiently accumulated in G_2, then accumulated in M and developed apoptosis from the mitotic cells (Fig. 6A). On the other hand, OVCAR-3 cells transiently accumulated in G_2 and M, part of them developed apoptosis from M, whereas other fraction progressed to a G_1' phase with double chromatin content and then developed apoptosis (Fig. 6B). However, when a similar experiment was performed with OVCAR-3 cells synchronized at G_1 by releasing them from a G_1-S thymidine block, the cells treated with FLUTAX from the G_1 or S phases developed apoptosis directly from mitosis, without significant accumulation of G_1'-double chromatin cells (Fig. 7A) (control cells without FLUTAX lost synchronization and became similar to control unsynchronized cells; not shown). 3T3.A31 non-transformed mouse fibroblast cells are more resistant to Taxol than U937 or OVCAR-3 cells (Table I). When these cells were synchronized in G_1 by releasing them from a G_0-G_1 arrest by serum deprivation and treated with FLUTAX, they transiently accumulated in G_2 and abnormal mitosis, and then proceeded to a cell cycle block at G_1' with double chromatin content (Fig. 7B). A similar result was obtained with unsynchronized cells. However, 3T3.A31 cells did not develop apoptosis within the time scale of the experiment (72 h), although these G_1' cells were characteristically micronucleated (see Fig. 5D) and presented fragmented centrosomes (see inset of Fig. 5D), clearly impaired by FLUTAX.

DISCUSSION

Centrosome and Spindle Microtubules Contain Cytotoxic Taxol Binding Sites, Imaged With Fluorescent Taxoid in Human Leukaemia Cells

The binding sites of FLUTAX at cytotoxic doses in U937 cells concentrate on the centrosome and spindle pole microtubules. Since the fluorescence microscopy images are erased with non-fluorescent taxoid, FLUTAX is known to be a specific probe of the Taxol binding site of microtubules [Evangelio et al., 1998; Díaz et al., 2000] and its effects fully parallel the cell cycle arrest and the apoptotic activity of Taxol (see Results), it can be concluded that the images presented here locate Taxol binding sites. This is, to our knowledge, a first direct imaging of the subcellular sites of specific binding of a cytotoxic microtubule drug in intact cells. The simplest interpretation is that the ligation of these binding sites is also a primary cause of cytotoxicity. The centrosomal labelling suggests that impairment of centrosome duplication or separation during interphase may subsequently result in abnormal mitosis and cell death (see below). The strong labelling of the microtubules near the spindle poles in mitosis indicates that FLUTAX is bound by microtubules growing from the spindle poles, most likely suppressing their dynamics. Consequently, these microtubules would probably not reach the equator, hence bipolar kinetochore attachment would be prevented, impairing the

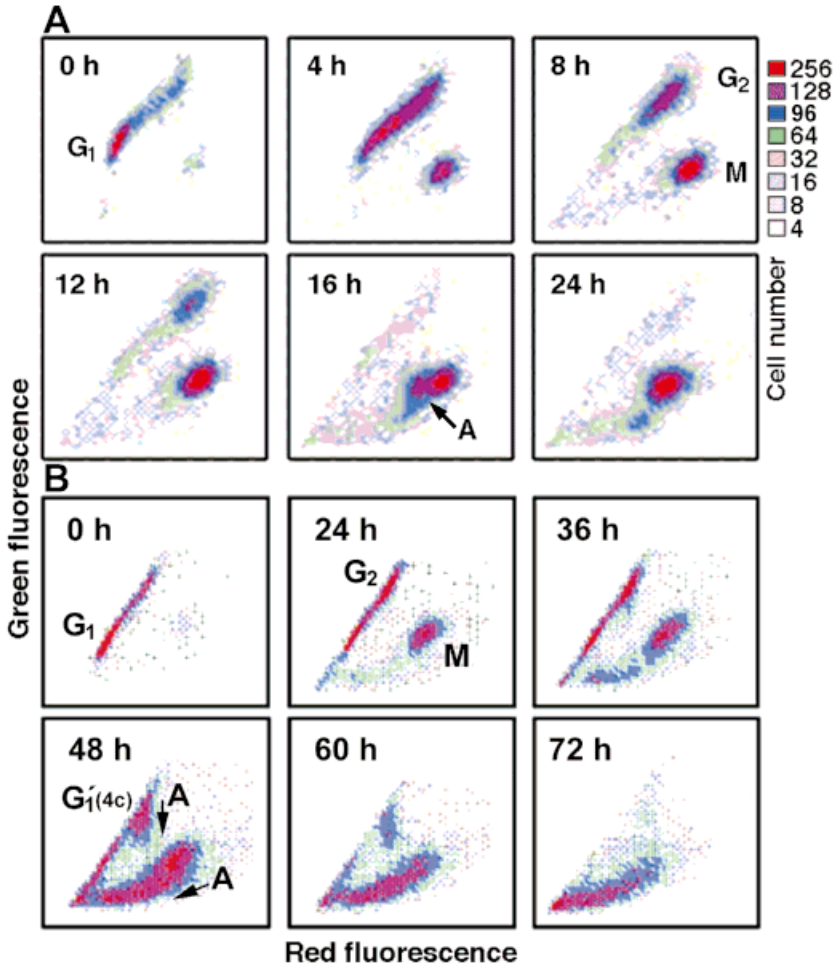

Fig. 6. Cell cycle of FLUTAX-treated U937 and OVCAR cells. **A:** Acridine orange flow cytometry of U937 treated with 90% growth inhibitory concentrations of FLUTAX (80 nM) during different periods of time. After extraction of RNA and partial acid denaturation of DNA, cellular double-stranded DNA shifts towards the green, while denatured single-stranded DNA shifts to the red with this metachromatic fluorochrome. The density distribution of cells in the green vs. red emission channels [Darzynkiewick, 1994] is indicated in each panel with a false colour scale shown (**right**). Peaks corresponding to cells in the different phases of the cell cycle and in apoptosis (A) are indicated. **B:** Acridine orange flow cytometry of OVCAR-3 cells treated with 150 nM FLUTAX (90% growth inhibition). Whereas U937 cells transiently accumulate in G_2 and M phases and then go into apoptosis (A), OVCAR-3 cells are hardly arrested in G_2, and they transiently accumulate in M and in abnormal G_1 with doubled DNA before undergoing apoptosis (B).

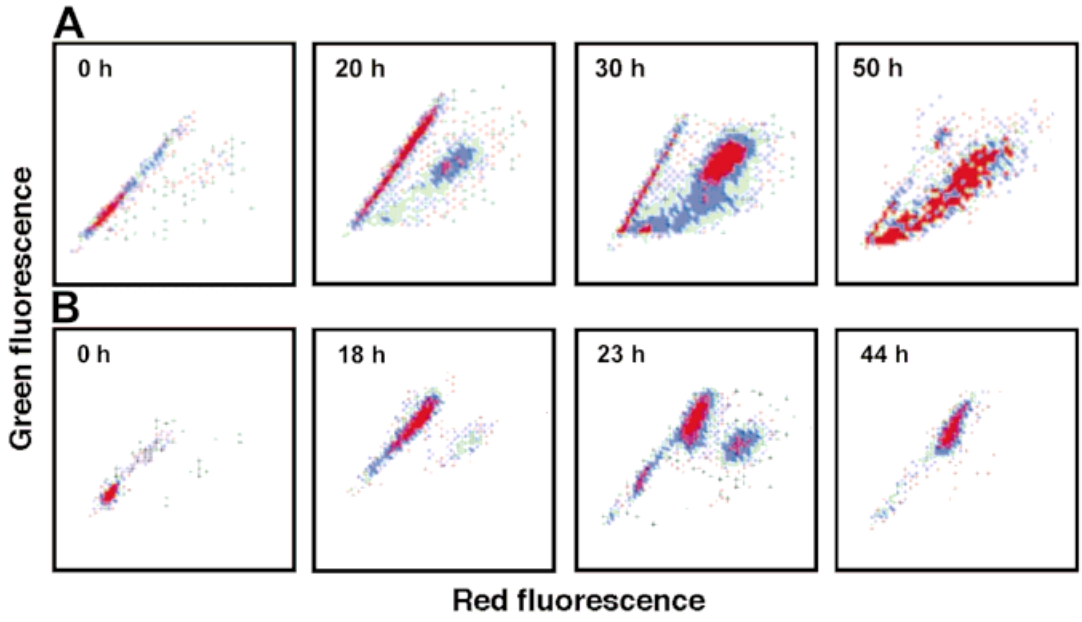

Fig. 7. Cell cycle evolution in FLUTAX-treated synchronized OVCAR-3 (**A**) and 3T3.A31 (**B**) cells. Acridine orange flow cytometry of OVCAR-3 and 3T3.A31 treated with 90% growth inhibitory concentrations of FLUTAX during different periods of time. OVCAR-3 cells were released from a G_1/S thymidine block and treated from G_1 phase (18 h after) with 375 nM FLUTAX during the indicated periods. DMSO controls were done in parallel at 20 and 50 h, when a loss of synchrony was observed; control cells not synchronyzed and treated with this drug concentration behaved as in Figure 6. 3T3.A31 cells were synchronized in G_0/G_1 by serum deprivation and treated from G_1 phase (6 h after serum addition) with 1 μM FLUTAX during the indicated times. DMSO controls made in parallel had a normal cell cycle (not shown).

metaphase to anaphase transition and triggering cell death.

Two important questions immediately arise: (1) why are mainly centrosomes labelled (Fig. 4A) more intensely than the whole microtubule network? and(2) why are spindle polar microtubules labelled (Fig. 4F) more than the rest of the spindle? We labelled permeabilized U937 cells with low FLUTAX concentrations in order to obtain a fluorescence intensity matching that of the labelled intact cells. Images resembling those of Figure 4A, but still showing cytoplasmic microtubules as in Figure 4D were obtained with 6 to 50 nM FLUTAX (not shown). Thus, a simple answer to the first question may be that the local concentration of taxoid binding sites in centrosomes is larger than in cytoplasmic microtubules, making these zones much brighter (it is unlikely that the spot labelling observed is a trivial consequence of the confluence of cytoplasmic microtubules in the centrosomal area; see Results). Alternative possibilities are that centrosomal components are binding FLUTAX more avidly than other microtubules. The high local concentration of cytotoxic taxoid bound by centrosomes is intriguing. The binding sites may be located at the centriolar β-tubulin, at very short nascent microtubules, or perhaps at the γ-tubulin rings, δ-tubulin, ϵ-tubulin, or in other components of the centrosomal complex [Zimmerman et al., 1999; Wiese and Zheng, 1999; Chang and Stearns, 2000], which can hardly be resolved with optical microscopy. Regarding the second question, the comparatively strong labelling of the spindle polar microtubules may be a simple consequence of a high local concentration of microtubules that are less brightly stained by immunofluorescence, since images similar to Figure 4F could be obtained with permeabilized U937 cells at low FLUTAX concentrations.

An interesting feature of FLUTAX-U937 cell binding and labelling of centrosomes and spindles, is its reversibility (Results; 6 to 9 h upon dilution in fresh medium, less than 4 h with an excess of non-fluorescent taxoid). Although Taxol binding to cellular microtubules has been frequently regarded as practically irreversible, this may depend on plasma membrane permeability and the particular conditions of the experiment, including the taxoid concentration. In fact, both FLUTAX and Taxol readily dissociate in minutes from PtK2 cytoskeletons and from in vitro assembled microtubules, easily attaining chemical equilibrium [Evangelio et al., 1998; Díaz et al., 1998, 2000]. This reversibility may facilitate the design of competition assays of binding to the Taxol site, such as the flow cytometry measurement of fluorescent taxoid uptake (Fig. 2A,B), the straightforward microscopical methods described (Fig. 4), and fluorescence anisotropy methods [Evangelio et al., 1998]. These fluorescence-based methods may be of help in the discovery of new antitumour compounds acting on the Taxol binding site [Bollag et al., 1995, ter Haar et al., 1996, Mooberry et al., 1999], or of hypothetical endogenous ligands of the Taxol binding site of microtubules [Schiff et al., 1979; Suffness 1994].

Centrosome and Microtubule Lesions Mark Pathways of Taxoid-Induced Cell Death

Characteristic lesions of the microtubule cytoskeleton could be directly imaged in this study with the same probe that induced them, differently from earlier results using indirect immunofluorescence. These lesions consisted of monopolar spindles and multiple asters, microtubule bundles, and impaired centrosomes. Monopolar spindles and multiple asters induced and visualized with FLUTAX constitute a marker of the taxoid-triggered cell death, since the abnormal mitotic tumour cells studied will die by apoptosis. Depending on the FLUTAX treatment, OVCAR-3 cells died either from abnormal mitosis or from a subsequent interphase with double chromatin content and micronuclei, while U937 cells died directly from aberrant mitosis.

The formation of microtubule bundles had been related with the Taxol sensitivity of different cells [Rowinsky and Donehower, 1995]. However, according to the observations reported here, the onset of monopolar spindles and multiple asters, which takes place earlier, may be a better marker of drug sensitivity. Thus, in the case of U937 cells FLUTAX-induced microtubule bundles are characteristic only of the last stages of cell death (note that we could not ascertain whether their bright fluorescence precedes apoptosis or is caused by massive FLUTAX entry after breaking of the plasma membrane, possibly correlated with a second stage of FLUTAX binding; see Fig. 2A). Microtubule bundles were observed at high doses of FLUTAX in treated OVCAR-3 cells, but again they were less conspicuous than the multiple asters, preceding them on the way to apoptosis.

The monopolar spindles and multiple asters indicate impairment of centrosome separation at the G_2-M transition. Monopolar spindles could result from failure of centrosomal separation before nuclear envelope breakdown. Instead of forming a bipolar spindle, microtubules would assemble around a single microtubule nucleation center, therefore forming monopolar spindles with the chromosomes attached to the periphery. Multiple asters should appear from spontaneous nucleation of microtubules. They were not the result of centrosome fragmentation, since a maximum of two dots per aster were stained with anti-γ-tubulin antibody. The observation that synchronized OVCAR cells treated with FLUTAX from the G_1 and S phases underwent apoptosis before reaching the next interphase suggests impairment of centrosome duplication. Untransformed 3T3.A31 cells

treated with FLUTAX from G_1 suffer centrosomal impairment and hence abnormal mitosis, although they are resistant to induction of apoptosis. This permits the visualization of multiple centrosomes with FLUTAX in the treated 3T3.A31 cells, which accumulate in micronucleated form; it also indicates a comparatively enhanced sensitivity of the OVCAR-3 cells to taxoid-induced centrosomal damage. Centrosome fragmentation could take place after an abnormal reorganization of the centrosome, at the time FLUTAX-induced asters progress through the mitotic block to a new interphase-like state without cell division.

The different patterns of cell cycle response to FLUTAX treatment indicate that the taxoid-treated cells may undergo a transient mitotic block, override the mitotic checkpoint forming multinucleated interphase cells that will end up in apoptosis [pathway I, $G_1 \rightarrow S \rightarrow G_2 \rightarrow M$ (transient block) $\rightarrow G_1' \rightarrow$ apoptosis] or alternately they may suffer a complete mitotic arrest, mitotic checkpoint activation, and proceed directly into apoptosis [pathwayII, $G_1 \rightarrow S \rightarrow G_2 \rightarrow M$(arrest) $\rightarrow$ apoptosis]. At the lower taxoid concentrations, minor centrosomal impairment may allow formation of bipolar spindles, albeit inhibition of microtubule dynamics will result in failure of correct chromosome segregation and catastrophic mitotic exit (pathway I). Centrosomal impairment was evidenced with docetaxel pulse treatment of HeLa cells in S and early G_2 phases, leading to dissociation of pericentriolar material from the centrioles, formation of two unequivalent asters at the onset of mitosis, and catastrophic mitotic exit with micronucleation [Paoletti et al., 1997]. The fact that the most frequent mitotic abnormalities observed here at cytotoxic taxoid concentrations were monopolar spindles and multiple asters indicates that impairment of centrosome separation at the G_2-M transition is a main cause of subsequent mitotic arrest (pathway II). This does not exclude a contribution from suppression of the spindle microtubule dynamics, manifested by detached chromosomes.

Activation of the mitotic checkpoint by impairment of centrosomes will directly lead to cell death from the mitotic block, probably via activation of the p34cdc2-cyclin B kinase [Donaldson et al., 1994, Shen et al., 1998], Raf-1 kinase [Torres and Horwitz, 1998] and Bcl-2 phosphorylation [Haldar et al., 1998, Srivastava et al., 1998; Fang et al., 1998]. The Raf-1/Bcl-2 mechanism of cell death operates at higher Taxol concentrations than death from aberrant mitosis in A549 cells [Torres and Horwitz, 1998]. Cells that pass through aberrant mitosis get into interphase with micronuclei and double chromatin content, and may proceed to apoptosis in a p53-dependent process [Woods et al., 1995; Wahl et al., 1996, Trielli et al., 1996]. Absence of the tumour suppressor protein p53, which surveys G_1 and spindle checkpoints in mice embryonic fibroblasts, results in abnormal centrosome amplification [Fukasawa et al., 1996]. While the role of p53 in the sensitivity of cancer cells to Taxol remains controversial, it is interesting that Taxol-resistant ovarian carcinoma cells with mutations in β-tubulin have non-functional p53, suggesting that this is an advantage in the development of Taxol-resistance [Giannakakou et al., 2000b]. Studying the correlation of the pattern of intracellular labelling by fluorescent taxoid in primary tumour cultures with their Taxol sensitivity, as well as their mechanisms of cell death, appears to be of potential interest in predicting the efficiency and cellular monitoring of Taxol chemotherapy.

In conclusion, the results presented in this study show that centrosomes contain cytotoxic Taxol binding sites, as detected with a fluorescent taxoid; taxoid binding results in centrosomal impairment and cell cycle de-regulation, and drives tumour cells to apoptosis. The localization of an increasing number of regulatory molecules to centrosomes points to the involvement of centrosomes in the control of mitotic entry and exit, in addition to nucleation and organization of microtubules [Zimmerman et al. 1999]. Centrosome inactivation has been described as part of a DNA-replication/DNA-damage control system, leading to the assembly of an anastral microtubule spindle and chromosome segregation failure in *Drosophila* embryos [Sibon et al., 2000]. Supernumerary disorganized centrosomes and genetic instability are characteristic of tumours, including human breast tumours [Lingle et al., 1998] and many other malignant tumours [Pihan et al., 1998], in support of Boveri's hypothesis of centrosome-induced tumorigenesis [Brinkley and Goepfert, 1998; Zimmerman et al., 1999]. It has been shown that the centrosome-associated kinase aurora2/STK15/AIK1 is amplified in multiple human cancers, probably resulting in centrosome amplification (which might be directly monitored with FLUTAX), aberrant spindle assembly, aneuploidy, and genetic instability [Bischoff et al., 1998; Zhou et al., 1998; Tanaka et al., 1999]. The present results open the perspective of antimitotic compounds acting on the cell cycle regulation through the spindle organizer, whose characteristic abnormalities in numerous tumours could represent sensitive targets for these drugs. Moreover, it might be hypothesized that the centrosomal taxoid binding sites are in fact regulatory binding sites of as yet undiscovered mitotic regulators.

ACKNOWLEDGMENTS

We thank Drs. I. Ringel and S.B. Horwitz for the gift of ^{3}H-Taxol, Dr. E. Quesada for his help in the synthesis of fluorescent taxoids, Dr. P. Draber and Dr. A. Wolff for the TU30 and GT335 monoclonal antibodies,

respectively. Thanks are due to Drs. F. Mollinedo, P. Aller, and A. Silva for discussions, M.A. Ollacarizqueta for help with CCD microscopy, and Dr. P. Lastres for flow cytometry and discussions. Taxol (paclitaxel) was in part a gift from Bristol-Myers-Squibb, Princeton, NJ, owner of the registered trade mark. Docetaxel (Taxotere) was a gift from Rhône-Poulenc Rorer, Antony, France.

REFERENCES

Andreu D, de la Viña S, Andreu JM. 1988. Chemical synthesis of five tubulin antigenic sequences. Intl J Peptide Protein Res 31:555–566.

Andreu JM, Bordas J, Díaz JF, Garcia de Ancos J, Gil R, Medrano FJ, Nogales E, Pantos E, Towns-Andrews E. 1992. Low resolution structure of microtubules in solution. Synchrotron X-ray scattering and electron microscopy of taxol-induced microtubules assembled from purified tubulin in comparison with glycerol- and Map-induced microtubules. J Mol Biol 226:169–184.

Andreu JM, Díaz JF, Gil R, de Pereda JM, García M, Peyrot V, Briand C, Towns- Andrews E, Bordas J. 1994. Solution structure of Taxotere-induced microtubules to 3 nm resolution. The change in protofilament number is linked to the binding of the taxol side chain. J Biol Chem 269:31785–31792.

Bhat N, Perera PY, Carboni JM, Blanco J, Golenbock DT, Mayadas TN, Vogel SN. 1999. Use of a photoactivable taxol analogue to identify unique cellular targets in murine macrophages: identification of murine CD18 as a major taxol-binding protein and a role for Mac-1 in taxol-induced gene expression. J Immunol 162:7335–7342.

Bischoff JR, Anderson L, Zhu Y, Mossie K, Ng L, Souza B, Schryver B, Flanagan P, Clairvoyant F, Ginther C, Chan CSM, Novotny M, Slamon DJ, Ploman GD. 1998. A homologue of Drosophila aurora kinase is oncogenic and amplified in human colorectal cancers. EMBO J 17:3052–3065.

Bobinnec Y, Moudjou M, Fouquet JP, Desbruyéres E, Edde B, Bornens M. 1998. Glutamylation of centriole and cytoplasmic tubulin in proliferating non-neuronal cells. Cell Motil Cytoskeleton 39:223–232.

Bollag DM, McQueney PA, Zhu J, Henses O, Koupal L, Liesch J, Goetz M, Lazarides E, Woods CM. 1995. Epothilones, a new class of microtubule-stabilizing agent with a Taxol-like mechanism of action. Cancer Res 55:2325–2333.

Bootsma D, Budke L, Vos O. 1964. Studies on synchronized divisions of tissue culture cells initiated by excess thymidine. Exp Cell Res 33:301–304.

Brinkley BR, Goepfert TM. 1998. Supernumerary centrosomes and cancer: Boveri's hypothesis resurrected. Cell Motil Cytoskeleton 41:281–288.

Campisi J, Morreo G, Pardee AB. 1984. Kinetics of G1 transit follownng brief starvation for serum factors. Exp Cell Res 152: 459–462.

Chang P, Stearns T. 2000. δ-Tubulin and ϵ-tubulin: two new human centrosomal tubulins reveal new aspects of centrosome structure and function. Nature Cell Biol 2:30–35.

Darzynkiewicz Z. 1994. Acid-induced denaturation of DNA in situ as a probe of chromatin structure. Methods Cell Biol 41:527–541.

De Brabander M, Geuens G, Nuydens R, Willebrords R, De Mey J. 1981. Taxol induces the assembly of free microtubules in living cells and blocks the organizing capacity of the centrosomes and kinetochores. Proc Natl Acad Sci USA 78:5608–5612.

Derry WB, Wilson L, Jordan MA. 1998. Low potency of Taxol at the minus ends: Implications for its antimitotic and therapeutic mechanism. Cancer Res 58:1177–1184.

De Inés C, Leynadier D, Barasoain I, Peyrot V, Garcia P, Briand C, Rener GA, Temple C Jr. 1994. Inhibition of microtubules and cell cycle arrest by a new 1-deaza-7,8- dihydropteridine antitumor drug, CI 980, and by its chiral isomer, NSC 613863. Cancer Res 54:75–84.

Díaz JF, Andreu JM. 1993. Assembly of purified GDP-tubulin into microtubules induced by Taxol and Taxotere: reversibility, ligand stoichiometry and competition. Biochemistry 32:2547–2755.

Díaz JF, Menendez M, Andreu JM. 1993. Thermodynamics of ligand-induced assembly of tubulin. Biochemistry 32:10067–10077.

Díaz JF, Andreu JM, Diakun G, Towns-Andrews E, Bordas J. 1996. Structural intermediates in the assembly of taxoid-induced microtubules and GDP-tubulin double rings: time-resolved X-ray scattering. Biophys J 79:2498–2420.

Díaz JF, Valpuesta JM, Chacón P, Diakun G, Andreu JM. 1998. Changes in microtubule protofilament number induced by taxol binding to an easily accessible site: internal microtubule dynamics? J Biol Chem 273:33803–33810.

Díaz JF, Strobe R, Engelborghs Y, Souto AA, Andreu JM. 2000. Molecular recognition of taxol by microtubules: kinetics and thermodynamics of binding of fluorescent taxol derivatives to an exposed site. J Biol Chem 275:26265–26276.

Donaldson KL, Goolsby G, Kiener PA, Wahl AF. 1994. Activation of p34cdc2 coincident with Taxol-induced apoptosis. Cell Growth Differ 5:1041–1050.

Evangelio JA, Abal M, Barasoain I, Souto AA, Lillo MP, Acuña AU, Amat-Guerri F, Andreu JM. 1998. Fluorescent taxoids as probes of the microtubule cytoskeleton. Cell Motil Cytoskeleton 39:73–90.

Fang G, Chang BS, Kim CN, Perkins C, Thompson CB, Bhalla KN. 1998. "Loop" domain is necessary for taxol-induced mobility shift and phosphorylation of Bcl-2 as well as for inhibiting taxol-induced cytosolic accumulation of cytochrome c and apoptosis. Cancer Res 58:3202–3208.

Fukasawa K, Choi T, Kuriyama R, Ruloong S, Vande Woude GF. 1996. Abnormal centrosome amplification in the absence of p53. Science 271:1744–1747 .

Giannakakou P, Sackett DL, Kang YK, Zhan Z, Buters JTM, Fojo T, Poruchynsky MS. 1997. Paclitaxel-resistant human ovarian cancer cells have mutant β-tubulins that exhibit impaired paclitaxel-driven polymerization. J Biol Chem 272:17118–17125.

Giannakakou P, Gussio R, Nogales E, Downing KH, Zaharevitz D, Bollbuck B, Poy GP, Sackett D, Nicolaou KC, Fojo T. 2000a. A common phamacophore for epothilone and taxanes: molecular basis for drug resistance conferred by tubulin mutations in human cancer cells. Proc Natl Acad Sci USA 97:2904–2909.

Giannakakou P, Poy G, Zhan Z, Knutsen T, Blagosklonny MV, Fojo T. 2000b. Paclitaxel selects for a mutant or pseudo-null p53 in drug resistance associated with tubulin mutations in human cancer. Oncogene 19:3078–3085.

Gonzalez-Garay ML, Chang L, Blade K, Menick DR, Cabral F. 1999. A β-tubulin leucine cluster involved in microtubule assembly and paclitaxel resistance. J Biol Chem 274:3875–23882.

Gorbsky GJ, Chen RH, Murray AW. 1998. Microinjection of antibody to Mad2 protein into mammalian cells induces premature anaphase. J Cell Biol 141:1193–1205.

Haldar S, Basu A, Croce CM. 1998. Serine-70 is one of the critical sites for drug induced Bcl2 phosphorilation in cancer cells. Cancer Res 58:1609–1615.

He L, Jagtap PG, Kingston, DGI, Shen HJ, Orr GA, Horwitz SB. 2000. A common pharmacophore for Taxol and the epothilones based on the biological activity of a taxane molecule lacking the C-13 side chain. Biochemistry 39:3972–3978

Horwitz SB. 1992. Mechanism of action of Taxol. Trends Pharm Sci 13:134–136.

Jimenez-Barbero J, Souto AA, Abal M, Barasoain I, Evangelio JA, Acuña AU, Andreu JM, Amat-Guerri F. 1998. Effect of 2′-OH acetylation on the bioactivity and conformation of 7-O-[N-(4′-fluoresceincarbonyl)-L-alanyl]taxol. A NMR-fluorescence microscopy study. Bioorg Med Chem 6:1857–1863.

Jordan MA, Wilson L. 1998. Microtubules and actin filaments: dynamic targets for cancer chemotherapy. Curr Opin Cell Biol 10:123–130.

Jordan MA, Toso RL, Thrower D, Wilson L. 1993. Mechanism of mitotic block and inhibition of cell proliferation by Taxol at low concentrations. Proc Natl Acad Sci USA 90:9552–9556.

Jordan MA, Wendell K, Gardiner S, Derry WB, Copp H, Wilson L. 1996. Mitotic block induced in HeLa cells by low concentrations of paclitaxel (Taxol) results in abnormal mitotic exit and apoptotic cell death. Cancer Res 56:816–825.

Lingle WL, Lutz WH, Ingle JN, Maihle NJ, Salisbury JL. 1998. Centrosome hypertrophy in human breast tumors: implications for genomic stability and cell polarity. Proc Natl Acad Sci 95:2950–2955

Long BH, Fairchild CR. 1994. Paclitaxel inhibits progression of mitotic cells to G_1 phase by interference with spindle formation without affecting other microtubule functions during anaphase and telophase. Cancer Res 54:4355–4361.

Long BH, Carboni JM, Wasserman AJ, Cornell LA, Casazza AM, Jensen PR, Lindel T, Fenical W, Fairchild CR. 1998. Eleutherobin, a novel cytotoxic agent that induces tubulin polimerization, is similar to paclitaxel (Taxol). Cancer Res 58:1111–1115.

Mollinedo F, Martinez-Dalmau R, Modolell M. 1993. Early and selective induction of apoptosis in human leukemic cells by the alkyl-lysophospholipid ET-18-OCH_3. Biochem Biophys Res Commun 192:603–609.

Monzó M, Rosell R, Sánchez JJ, Lee JS, O'Brate A, Gonzalez-Larriba JL, Alberola V, Lorenzo JC, Núñez L, Ro JY, Martín C. 1999. Paclitaxel resistance in non-small-cell lung cancer associated with β-tubulin gene mutations. J Clin Oncol 17:1786–1793.

Mooberry Sl, Tien G, Hernandez AH, Plubrukarn A, Davidson BS. 1999. Laulimalide and isolaulimalide, new paclitaxel-like microtubule-stabilizing agents. Cancer Res 59:653–660.

Nogales E, Wolf SG, Downing K. 1998. Structure of the αβ-tubulin by electron crystallography. Nature 391:199–203.

Nogales E, Whittaker M, Milligan RA, Downing KH. 1999. High-resolution model of the microtubule. Cell 96:79–88.

Nováková M, Dráverová E, Schürman W, Czihak G, Viklický V, Draber P. 1996. γ-tubulin redistribution in taxol-treated mitotic cells probed by monoclonal antibodies. Cell Motil Cytoskeleton 33:38–51.

Ojima I, Chakravarty S, Inoue T, Lin S, He L, Horwitz SB, Kuduk SD, Danisjefsky SJ. 1999. A common pharmacophore for cytotoxic natural products that stabilize microtubules. Proc Natl Acad Sci USA 96:4256–4261.

Paoletti A, Bornens M. 1997. Organisation and functional regulation of the centrosome in animal cells. Prog Cell Cycle Res 3:285–299,

Paoletti A, Giocanti N, Fauvaudon V, Bornens M. 1997. Pulse treatment of interphasic HeLa cells with nanomolar doses of docetaxel affects centrosome organization and leads to catastrophic exit of mitosis. J Cell Sci 110:2403–2415.

Parness J, Horwitz SB. 1981. Taxol binds polymerized tubulin in vitro. J Cell Biol 91:479–487.

Pihan GA, Purohit A, Wallace J, Knecht H, Woda B, Quesenberry P, Doxsey SJ. 1998. Centrosome defects and genetic instability in malignant tumors. Cancer Res 58:3974–3985.

Rao S, Krauss NE, Heerding JM, Orr GA, Horwitz SB. 1994. 3′-(p-azidobenzamido) taxol photolabels the N-terminal 31 aminoacids of β-tubulin. J Biol Chem 269:3132–3134.

Rao S, Orr GA, Chaudhary AG, Kingston DGI, Horwitz SB. 1995. Characterization of the Taxol binding site on the microtubule. 2-(m-azidobenzoyl) taxol photolabels a peptide (amino acids 217-231) of beta-tubulin. J Biol Chem 270:20235-20238.

Rao S, He L, Chakravarty S, Ojima, I, Orr GA, Horwitz SP. 1999. Characterization of the taxol binding site on the microtubule. Identification of arg(282) in beta-tubulin as the site of photoincorporation of a 7-benzophenone analogue of taxol. J Biol Chem 274:37990–37994.

Rodi DJ, James RW, Sanganeee HJ, Holton RA, Wallace BA, Makowski L. 1999. Screening of a library of phage displayed peptides identifies human bcl-2 as a taxol-binding protein. J Mol Biol 285:197–203.

Rowinsky EK, Donehower R. 1995. Paclitaxel (Taxol). New Engl J Med 332:1001–1014.

Schiff PB, Fant J, Horwitz SB. 1979. Promotion of microtubule assembly in vitro by Taxol. Nature 277: 665–667.

Schiff PB, Horwitz SB. 1980. Taxol stabilizes microtubules in mouse fibroblast cells. Proc Natl Acad Sci USA 77:1561–1565.

Shen SC, Huang TS, Jee SH, Kuo ML. 1998. Taxol-induced p32cdc2 kinase activation and apoptosis inhibited by TPA in human breast MCF-7 carcinoma cells. Cell Growth Differ 9:23–29.

Sibon OCM, Kelkar A, Lemstra W, Theurkauf WE. 2000. DNA-replication/DNA-damage-dependent centrosome inactivation in Drosophila embryos. Nature Cell Biol 2:90–95.

Sorger PK, Dobles M, Tournebize R, Hyman AA. 1997. Coupling cell division and cell death to microtubule dynamics. Curr Opin Cell Biol 9:807–814

Souto AA, Acuña AU, Andreu JM, Barasoain I, Abal M, Amat-Guerri F. 1995. New fluorescent water-soluble taxol derivatives. Angew Chem Int Ed Engl 34:2710–2712.

Srivastava RK, Srivastava AR, Korsmeyer SJ, Nesterova M, Cho-Chung YS, Longo DL. 1998. Involvement of microtubules in the regulation of Bcl2 phosphorylation and apoptosis through cyclic AMP-dependent proteinkinase. Mol Cell Biol 18:509–3517.

Suffness M. 1994. Is Taxol a surrogate for a universal regulator of mitosis? In Vivo 8:867–878.

Suffness M, editor. 1995. Taxol, science and applications. Boca Raton, FL: CRC Press. 496 p.

Tanaka T, Kimura M, Matsunaga K, Fukada D, Mori H, Okano Y. 1999. Centrosomal Kinase AIk1 is overexpressed in invasive ductal carcinoma of the breast. Cancer Res 59:2041–2044.

Ter Haar E, Kowalsky RJ, Lin CM, Longley RE, Gunasekera SP, Rosenkranz HS, Day BW. 1996. Discodermolide, a cytotoxic marine agent that stabilizes microtubules more potently than Taxol. Biochemistry 35:243–250.

Torres K, Horwitz SB. 1998. Mechanisms of Taxol-induced cell death are concentration dependent. Cancer Res 58:3620–3626.

Trielli M O, Andreassen PR, Lacroix FB, Margolis RL. 1996. Differential Taxol- dependent arrest of transformed and nontransformed cells in the G_1 phase of the cell cycle, and specific-related mortality of transformed cells. J Cell Biol 135:689–670.

Wahl AF, Donaldson KL, Fairchild C, Lee FYF, Foster SA, Demers GW, Galloway DA. 1996. Loss of normal p53 function confers sensitization to Taxol by increasing G_2/M arrest and apoptosis. Nature Med 2:72–79.

Waters JC, Chen RH, Murray AW, Salmon ED. 1998. Localization of Mad2 to kinetochores depends on microtubule attachment, not tension. J Cell Biol 141:1181–1191.

Wiese C, Zheng Y. 1999. γ-Tubulin complexes and their interaction with microtubule- organizing centers. Curr Opin Struct Biol 9:250–259.

Wolff A, de Nechaud B, Chillet D, Mazarguil H, Desbruyeres E, Audebert S, Edde B, Gros F, Denoulet P. 1992. Distribution of glutamylated alpha and beta-tubulin in mouse tissues using a specific monoclonal antibody, GT335. Eur J Cell Biol 59:425–432.

Wolfson M, Yang CPH, Horwitz SB. 1997. Taxol induces tyrosine phosphorylation of Shc and its association with Grb-2 in murine RAW 264.7 cells. Int J Cancer 70:248–252.

Woods C, Zhu J, McQueney PA, Bollag D, Lazarides E. 1995. Taxol-induced mititic block triggers rapid onset of a p53-independent apoptotic pathway. Mol Med 1:506–526.

Yvon A-M, Wadsworth P, Jordan MA. 1999. Taxol suppresses dynamics of individual microtubules in living human tumor cells. Mol Biol Cell 10:947–959.

Zhai Y, Kronebusch PJ, Simon PM, Borisy GG. 1996. Microtubule dynamics at the G_2/M transition: abrupt breakdown of cytoplasmic microtubules at nuclear envelope breakdown and implications for spindle morphogenesis. J Cell Biol 135:204–214.

Zhou H, Kuang J, Zhong L, Kuo W, Gray JW, Sahin A, Brynkley BR, Shen S. 1998. Tumor amplified kinase STK15/BTAK induces centrosome amplification, aneuploidy and transformation. Nature Genet 20:189–192.

Zimmerman W, Sparks CA, Doxey SJ. 1999. Amorphous no longer: the centrosome comes into focus. Curr Opin Cell Biol 11:122–128.